Robust Non-Linear Control of Hybrid Super Capacitor based EV Charger for grid to vehicle and vehicle to grid Application

By

Eram Bushra

Fall-2021-MS-EE 00000361453 SEECS

Supervisor

Dr. Iftikhar Ahmad Rana

Department of Electrical Engineering

A thesis submitted in partial fulfilment of the requirement for the degree of Master of Science in Electrical Engineering (MS-EE)

In

School of Electrical Engineering &Computer Science (SEECS),

National University of Science and Technology (NUST),

Islamabad, Pakistan

(May 2023)

THESIS ACCEPTANCE CERTIFICATE

Certified that final copy of MS/MPhil thesis entitled "Robust Non-Linear Control of Hybrid Super Capacitor based EV Charger for grid to Vehicle and vehicle to grid Applications" written by Eram Bushra Bushra, (Registration No 361453), of SEECS has been vetted by the undersigned, found complete in all respects as per NUST Statutes/Regulations, is free of plagiarism, errors and mistakes and is accepted as partial fulfillment for award of MS/M Phil degree. It is further certified that necessary amendments as pointed out by GEC members of the scholar have also been incorporated in the said thesis.

Signature: _____

Name of Advisor: Dr. Iftikhar Ahmad Rana

Date: _____17-Apr-2023_____

HoD/Associate Dean:_____

Date: _____
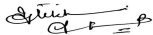
Signature (Dean/Principal): _____

Date: _____

ii

Approval

It is certified that the contents and form of the thesis entitled "Robust Non-Linear Control of Hybrid Super Capacitor based EV Charger for grid to Vehicle and vehicle to grid Applications" submitted by Eram Bushra Bushra have been found satisfactory for the requirement of the degree

Advisor :   Dr. Iftikhar Ahmad Rana

Signature: _____

Date: _____ 17-Apr-2023 _____

Committee Member 1:Dr. Ammar Hasan

Signature: _____

18-Apr-2023

Committee Member 2:Dr. Usman Ali

Signature: _____

Date: _____ 17-Apr-2023 _____
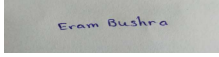
Signature: _____

Date: _____

ii

Dedication

I would like to dedicate my thesis to my beloved parents for their endless affection, support, and assistance throughout during my education. Their endless efforts helped me to have a key to unleash the mysterious of the world. I wish this accomplishment will fulfil the dream they imagined for me.

Certificate of Originality

I hereby declare that this submission titled "Robust Non-Linear Control of Hybrid Super Capacitor based EV Charger for grid to Vehicle and vehicle to grid Applications" is my own work. To the best of my knowledge it contains no materials previously published or written by another person, nor material which to a substantial extent has been accepted for the award of any degree or diploma at NUST SEECS or at any other educational institute, except where due acknowledgement has been made in the thesis. Any contribution made to the research by others, with whom I have worked at NUST SEECS or elsewhere, is explicitly acknowledged in the thesis. I also declare that the intellectual content of this thesis is the product of my own work, except for the assistance from others in the project's design and conception or in style, presentation and linguistics, which has been acknowledged. I also verified the originality of contents through plagiarism software.

Student Name:Eram Bushra Bushra

Student Signature:

Acknowledgements

Contents

List of Figures

List of Tables

Abstract

The goal of this work is to design a Super Twisting Sliding Mode Controller (ST-SMC), a robust nonlinear controller technique for electric vehicle (EV) charging systems. In this work, a hybrid supercapacitor (HSC) has been employed as a storage mechanism. Since recent years, hybrid supercapacitors have gained popularity due to their enhanced energy density performance without affecting their power density. The lithium-ion capacitor (LIC) is the advanced hybrid energy storage system that offers benefits such as high energy and power densities, long cycle lives, and a wide range of temperature for operation. Utilising specified fast-charging points and averting full and longer charges, LIC can be employed with Opportunity (OP) charging for an EV during the operation phase. The Grid to vehicle (G2V) and vehicle to grid (V2G) strategies can both use electric vehicle (EV) chargers to effectively connect the grid and the vehicle in a two-way manner. The control of power flow is a difficult task in either of the setups, though. The bi-directional power converter in a BEV charger is controlled by a controller ST-SMC, which tracks the charger's intended current and output voltage in both G2V and V2G operations. A significant weakness in power converters is the chattering effect, which is mitigated by the suggested controller. For the comparison, the robust integral backstepping sliding mode controller (IBS-SMC) is also developed. The Lyapunov stability method is used to examine the system's stability. In the MATLAB/Simulink software, the suggested controllers are simulated. Results confirm the controller's effectiveness under different operating circumstances.

CHAPTER 1

1   Introduction

The main challenge in current world is need for effective storage of energy and sustainable energy options. The devices that can store energy like supercapacitors, fuel cells, and some other devices can be used to meet this need. The equipment devoted to storing energy particularly is called a supercapacitor [1]. They can provide enough energy and the power densities geared towards low to high power ensuing objectives. These are some storage items that can be considered between typical capacitors and batteries [2]. Many other technologies have come up to ease the major concerns over energy problem [3]. The technologies' primary goal is to lessen greenhouse gas contamination brought on by usage of the fossil fuels [4]. Supercapacitors are one of the options, that can provide high power densities, longer cycle lives, faster charging, and discharging times, and a secure method of electrochemical energy storage [5].

According to the storage criteria, supercapacitors are divided into the three main categories: one is EDLC, second is pseudo capacitor, and third one is hybrid supercapacitor. Energy storage of supercapacitor is based on the cumulation of charge. Batteries, fuel cells, and the supercapacitors are examples of unconventional energy storage systems that rely on electrochemical reactions. Supercapacitors have extended charging and discharging cycles and a wide working range of temperature, which makes them preferable to batteries and fuel cells [6]. The devices thar have highest capacitance and highest energy storage capacity are hybrid supercapacitors (HSC). Because of propensity to combine properties of their constituent parts (EDLC and pseudo capacitor), they are attracted a lot of attention [7].

There are many potential combinations, but those created by conducting and electroactive elements with an eye towards energy storage are of particular interest [8]. The HSC, which is the EDLC, and pseudo capacitor combined, has improved properties over the combining parts. The shell area and atomic charge length serve as the foundation for energy storage in EDLC [9]. Whereas in the pseudo capacitor, energy storage is attained via fast, repetitive reactions between electroactive resting on active electrode and the electrolyte solution [10]. The mechanism of energy storage in hybrid supercapacitors is consisted of the two storage systems together. The HSC functions as the EDLC in one side and as the pseudo capacitor in the other. By comparing to the standard EDLC and the pseudo capacitor, HSC have high power and energy densities. This encourages their adoption in systems that utilise less energy than other

energy-storing devices. However, HSC reach the pinnacle of power density when compared to fuel cells and batteries while having a significantly lower power density when compared to regular capacitors [11].

Supercapacitors' constantly improving performance causes an increase in the applications for them. The batteries that can be recharged have mostly high demand in the energy storage industry for the past 10 years. The need for better energy storage is rising quickly for a variety of applications related to electronic portability for hybrid electric cars [12]. Specially in the sphere of hybrid energy vehicles, the use of hybrid supercapacitors is expanding. Electric vehicles (EVs) can use hybrid supercapacitors as a single source; however, it depends on the needs of the vehicle and its intended use case. The energy storage capacities of a supercapacitor and a battery are combined in a hybrid supercapacitor. In order to create a single device that has the ability to deliver both high energy density and high output, two different energy storage technologies, such as a high-capacity battery and a high-power supercapacitor, are combined under the umbrella term "hybrid." When compared to either a battery or a supercapacitor by themselves, this combination offers better performance and a longer lifespan [13].

There are a few examples of the several types of electric cars (EVs). Each model has unique features, such as the HEV's use of both the internal combustion engine (ICE) and the electric motor, which means it emits some bad gasses, the PHEV's high efficiency and need for an external source to recharge the batteries in a PHEV, the BEV's short range, and the FHEV, which has been proposed as a solution to all the problems mentioned above but is somewhat expensive [14].

The primary component of HEVs, which powers the traction motor, is the hybrid energy storage system (HESS). FHEVs use various fuel cell, battery, and supercapacitor combinations because fuel cells alone cannot handle the required load [15]. In [16], HESS based on fuel cells and supercapacitors has been suggested for HEV. Similarly in the way the combo of fuel cell and battery is considered in [17]. According to a comparison research, HESS consisting of fuel cell, battery and super-capacitor represents a more practical solution because battery and the supercapacitor alone are unable to satisfy the needs of a superior HESS [18]. In [19], three different power sources are part of HESS, which has been suggested. This model has larger storage space and a high-power density.

Since hybrid supercapacitors can be utilised for Vehicle-to-Grid (V2G) applications just like batteries, EVs may be viewed as "mobile power banks." EVs are employed in the idea of V2G as a mobile energy storage system to supply the grid during periods of high demand or when renewable energy sources are not accessible. Because they have a longer life cycle than batteries and can be charged and discharged quickly, supercapacitors are particularly well suited for V2G applications. Supercapacitors' high-power density enables them to swiftly deliver electricity to the grid at times of peak demand, and their quick energy storage and release helps them to balance out the variability of renewable energy sources. Due to their suitability for V2G applications, hybrid supercapacitors [20].

Power exchange that is effective requires DC-DC power converters. For HEVs, many converter configurations have been covered in [21]. In [22] it has been suggested how to create a device that interleaved DC-DC converter for HEVs. In [21], each power source is connected to the DC-DC converter using a multiple converter topology.

Soon, the concept of V2X, which transmits power from a hybrid supercapacitor to the infrastructure, will become more well-known [23]. V2X refers to power flow from automobiles to some other devices, and as illustrated in Fig. 1, this power flow might be from a V2L, a V2H, or V2G.
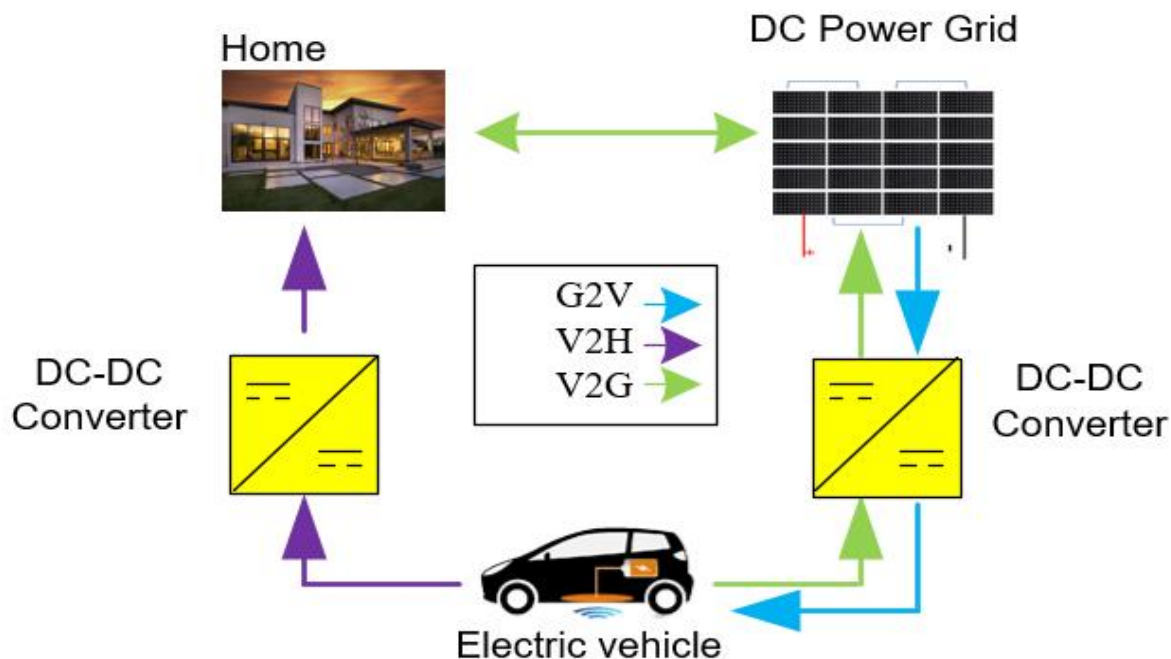

Figure 1. 1: Flow of Power in V2X *[24]*

V2L is designed to instantly transmit electricity from a vehicle to an appliance in the event of an emergency. The objectives of the management, the power distribution control, and the stability of grid power in the outage, the technology V2H and V2G technology are being deployed [25]. Electric vehicle chargers can be categorised into two groups: one is conductive and the other one is inductive, depending on the method of power transmission. Additionally, they are separated into the unidirectional and the bidirectional chargers. To support V2X technologies, the converter must be bidirectional and have an appropriate power rating [26]. In V2G technology, the energy from the vehicle hybrid supercapacitor is transmitted to the grid, but in V2H technology, the energy is sent to the loads in the home. DC-DC converter that is reversible runs in buck mode while the bidirectional AC-DC converter performs as a rectifier with sinusoidal current absorption in G2V mode. On the other hand, DC-DC converter that is reversible operates in the boost mode, AC-DC converter works as an inverter in the V2G working mode [27].

For the energy management of energy storage systems (ESS), a variety of control mechanisms have been developed. In [28], for effective power management of ESS, the fuzzy logic and the optimised neural network control methods are proposed. Battery/supercapacitor-based ESS has been suggested using a model predictive control method in [29]. For FC-SC based HESS, BS and BS-SMC have recently been developed [30]. In [31], For HESS with many sources, AT-SMC has been used. However, no car specifications are considered in this analysis. Because of the nonlinear behaviour of power converters, a bi-linear model of fuel cell, SC and battery-based HESS is created, and a Lyapunov-based nonlinear controller is designed to meet desired

objectives [32]. In [33], DISMC has been developed and researched for solar power systems. SMC, ISMC, along with DISMC have been addressed in [34].

1.1   Problem Statement and Contribution

A strong nonlinear controller must be created to control the voltage at output of the EV charger and chase the desired currents in the G2V and the V2G in the existence of the external disturbances with less chattering. To control the numerous applications in diverse works, ST-SMC is utilised [35] and it entails switching control's continuous approximation. In order to achieve the control goals, ST-SMC is proposed in this research, with the control signal being changed into the duty cycles using a PWM. The main contributions of this study are as follows:

- A robust nonlinear higher order sliding mode controller (ST-SMC) has been developed in contrast to many of linear controllers found in literature.
- Chattering's impact has been minimised, reducing the system's heat and power losses.
- The system's dynamic reaction has increased, which is essential for enhancing the operational needs of the G2V and V2G modes.
- Analysis of the settling time, rising time, peak value, and chattering effect is done by simulation.

1.2   Sliding Mode Controller (SMC)

A reliable nonlinear controller, SMC has advantage such as finite time convergence, low steady error, minimal computing cost, and ease of implementation. The choice of the sliding surface is made in the phase, and the control rule is then developed in a way that will point the system in the direction of the sliding surface. A graphic representation of SMC is shown in Fig. 2. It demonstrates how the variable initially has a value of Xo and then, because of control action, converges to sliding surface and finally reaches intended value [34].

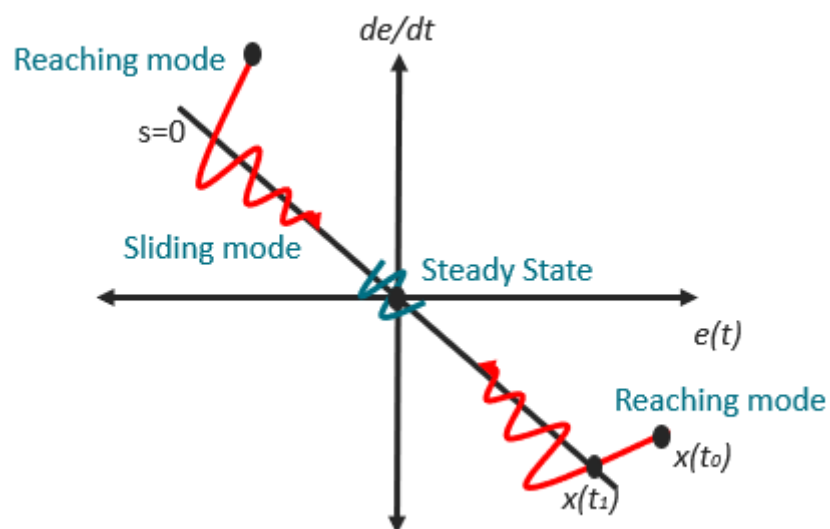In this study, the designs of ST-SMC and IBS-SMC have been compared based on their findings.

Figure 1. 2: Sliding Mode Control *[34]*

Chapter 2

2   Literature Review

Most of the linear controllers, including proportional integral controllers and the linear quadratic optimal controllers, are used to regulate the charging units for EVs [36], have been put forth in the paper. The PI controller [37] has suggested creating the EV charger using the SEPIC. Such controllers are made to govern the converter's dynamics in the EV charger. These controllers have better dynamic performance, but they can only operate at the operating point where system is linearized. Additionally, these are not resistant to outside perturbations. Soft computing controllers are also created in the literature. In [38], To manage the speed profile of an EV, a fuzzy PI controller for a multi-input DC-DC converter has been developed. Additionally, a fuzzy logic-based controller for the EV charger has been suggested [39], which is based on human thinking and does not call for the usage of a mathematical model. Each control variable has a membership function applied to it with a value ranging from 0 to 1. Their efficacy is reliant on accurate system information being available, which isn't always the case. Likewise, several database strategies have been used in contemporary publications [40] for a variety of applications, including electric vehicles, methods for estimating the health of batteries are described; however, these methods rely on data and do not take into account the nonlinear regulation of G2V and the V2G processes.

To manage non-linear dynamics of EV charger, numerous nonlinear controllers have also been created. Output Feedback controller [41] is suggested for DC-DC converter; nevertheless, it does not properly demonstrate dynamic performance. It guarantees system's overall asymptotic stability. Additionally, it is not resistant to outside perturbations. Backstepping (BS) has been recommended [42] for the dynamic performance-enough regulation of the power converters in the EV charging device. However, it is not resistant to outside disturbances and exhibits some steady state inaccuracy. Control strategy of BS is strengthened to face external disturbances by addition of a switching control rule, but at expense of the chattering, that results in heat losses and the power losses in system.

All these controllers' principal drawbacks are that they lack robustness against external disturbances and fail to guarantee finite-time convergence to the intended trajectories. A SMC-IBS [43] has been created for managing AC-DC converter's dynamics in the EV charger. Compared to other controllers, these controllers have greater dynamic performance and finite time convergence. In [44], It is suggested to use an sliding mode-based charger controller that

is resistant to sorts of uncertainty and disruption. The fundamental drawback of the sliding mode controller, on the other hand, is that sliding trajectory exhibits chattering effect [45].

Chapter 3

3   System Model and Mathematical Modelling

3.1   System Model

It is assumed that the system's power conversion unit is operating. The following full derivation, however, illustrates a variety of modes of power conditioning circuitry:

3.1.1   Description of the system

Fig. 3.1 depicts the overall block diagram of converter. Controller block, that produces the control signal U, receives input from the converter states h1, h2, and h3.
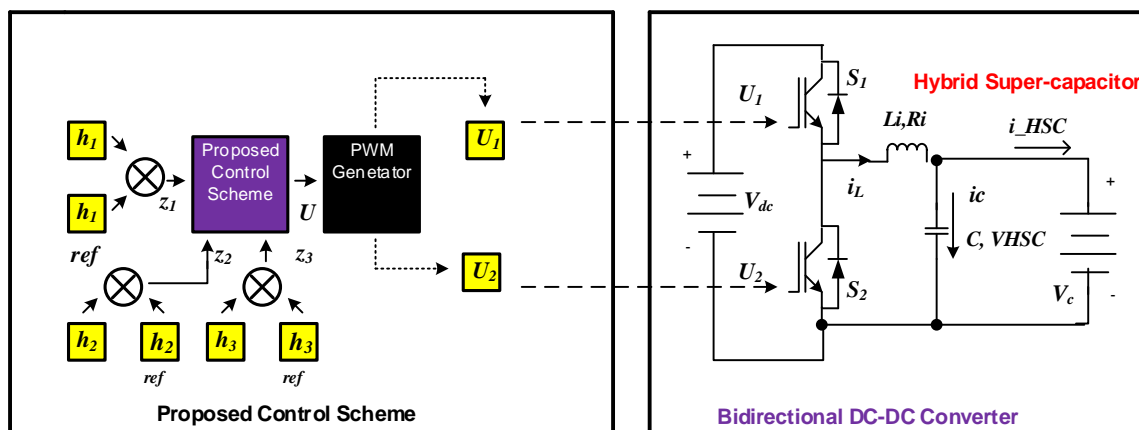

Figure 3. 1: Bidirectional DC-DC Power Converter with control scheme *[24]*

Figure. 3.1 shows the bidirectional DC-DC converter coupled to the hybrid supercapacitor. [46]. With its two switches S1, S2, filtering inductance Li, and capacitance C, this converter functions like a half bridge. Figure 3.2 displays internal resistance Ri and inductance Li.
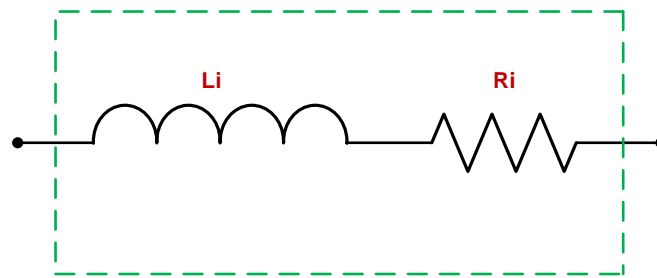
Figure 3. 2: Internal Resistance with inductor *[24]*

The converter's output voltage is utilised to charge the HSC, or hybrid supercapacitor.

3.2 Modelling of the System

3.2.1 Hybrid Supercapacitor

The converter's output voltage is utilised to charge the HSC, or hybrid supercapacitor. In the G2V operation mode, this converter functions as a buck converter. During the charging stage, it is employed to regulate the HSC current and voltage. To ensure smooth operation while in V2X, the converter works like boost converter to increase the HSC voltage to a [47]. Figure. 4 shows the electrical circuit of the HSC. The capacitance of the HSC is C_{HSC}.

Figure 3. 3: Hybrid supercapacitor (LIC) Electric Model *[47]*

3.2.2 Bidirectional DC-DC Converter

During V2G and G2V, this converter functions in the following modes.

3.2.2.1 Buck Mode

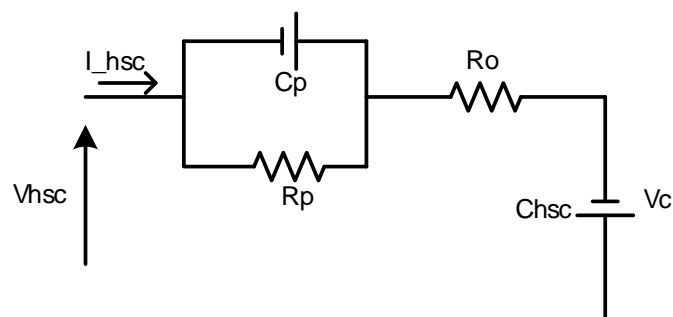PWM signal U1 controls the switch S1, while the switch S2 is left open for a duty cycle U2 of zero. The charger's DC output link then sends the electrical energy to HSC. In this mode of operation, the converter reduces the charger's output voltage to the level needed to charge the battery. G2V mode will be used for system operation overall. Figure. 5 shows electrical circuit for the converter.
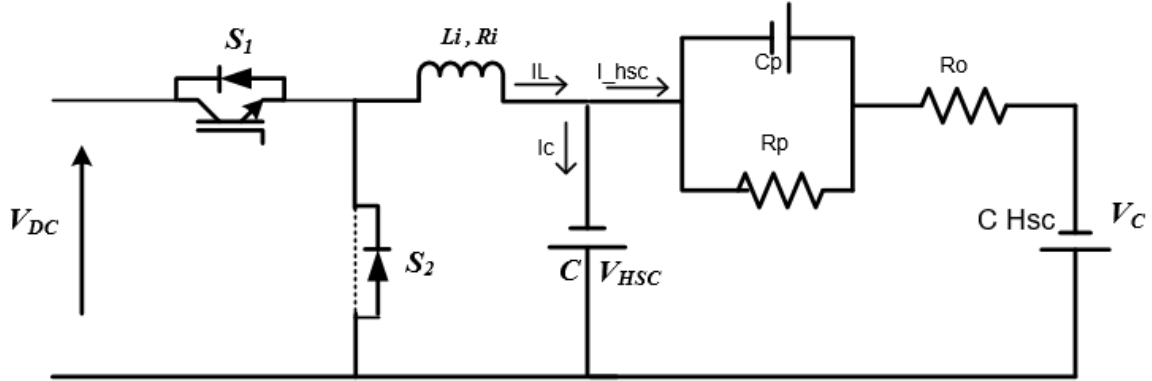
Figure 3. 4: Buck Mode of operation

The switching model shown in the following diagram can be created:

$$Li\frac{dI_L}{dt} = -RiI_L - V_{HSC} + U_1 V_{DC} \qquad (1)$$

$$C\frac{dV_{HSC}}{dt} = I_L - \frac{1}{R_O}V_{HSC} + \frac{1}{R_O}V_C \qquad (2)$$

$$C_{HSC}\frac{dV_C}{dt} = \frac{1}{R_O}V_{HSC} - \frac{1}{R_O}V_C \qquad (3)$$

3.2.2.2 Boost Mode

The switch S1 is left open while U1 is equal to zero and the switch S2 is kept off throughout U2's duty cycle. The HSC transmits its energy to the DC bus. In this working mode, the HSC voltage will be increased to the necessary voltage value using the DC-DC converter, and the entire system will run in V2G mode. Fig. 6 shows the converter's appropriate electrical circuit in this scenario.
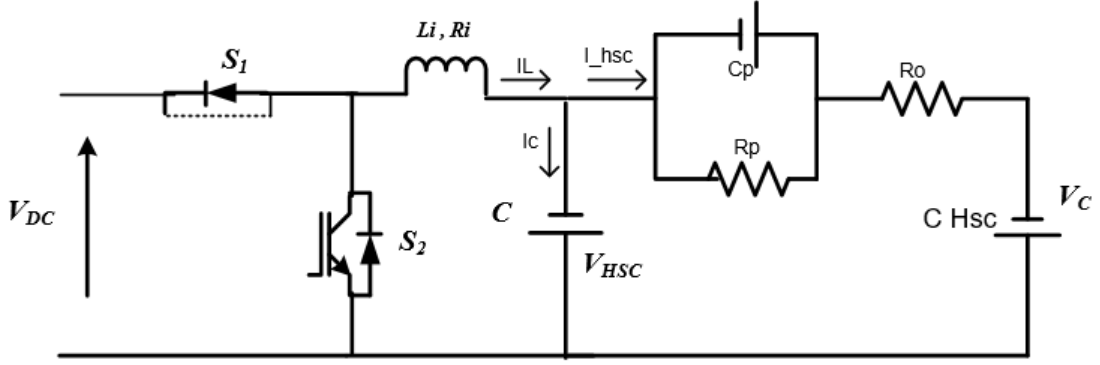
Figure 3. 5: Boost mode of operation

By solving the above model:

$$Li\frac{dI_L}{dt} = -RiI_L - V_{HSC} + (1 - U_2)V_{DC} \tag{4}$$

$$C\frac{dV_{HSC}}{dt} = I_L - \frac{1}{R_O}V_{HSC} + \frac{1}{R_O}V_C \tag{5}$$

$$C_{HSC}\frac{dV_C}{dt} = \frac{1}{R_O}V_{HSC} - \frac{1}{R_O}V_C \tag{6}$$

3.2.2.3 Bidirectional Mode

The state space equations are:

$$Li\frac{dI_L}{dt} = -RiI_L - V_{HSC} + \omega V_{DC} \tag{7}$$

$$C\frac{dV_{HSC}}{dt} = I_L - \frac{1}{R_O}V_{HSC} + \frac{1}{R_O}V_C \tag{8}$$

$$C_{HSC}\frac{dV_C}{dt} = \frac{1}{R_O}V_{HSC} - \frac{1}{R_O}V_C \tag{9}$$

Where

$$\omega = (TU_1 + (1 - T)(1 - U_2)) \tag{10}$$

T is a parameter that is affected by the DC-DC converter's working modes.

- If T = 1 then it is buck mode
- If T = 0 then it is boost mode

Equations (7) through (9), which reflect the typical mathematical modelling of a DC-DC converter, are given below.

$$\dot{h_1} = -\frac{R_i}{L_i}h_1 - \frac{1}{L_i}h_2 + \omega\frac{V_{DC}}{L_i} + d(t) \tag{11}$$

$$\dot{h_2} = \frac{h_1}{C} - \frac{1}{CR_O}h_2 + \frac{h_3}{R_O C} \tag{12}$$

$$\dot{h_3} = \frac{h_2}{R_O C_{HSC}} - \frac{h_3}{R_O C_{HSC}} \tag{13}$$

Where $\dot{h_1}$ indicates the average inductor current I_L, $\dot{h_2}$ and $\dot{h_3}$ denote the average output voltage V_{HSC}. The disturbance $d(t)$ has been included in the system, whose bounds are as follow:

$$B_1 \leq d(t) \geq B_2 \tag{14}$$

B_1 is lower disturbance and B_2 is upper disturbance.

$$\dot{h_2} = \frac{h_1}{C} - \frac{1}{CR_O}h_2 + \frac{h_3}{R_O C}$$

Chapter 4

4 Controller Design

The single CC process with the negative current reference during V2G mode. The following goals are intended to be attained by the resilient nonlinear controllers:

- To provide consistent voltage and current management
- To guarantee steady current and voltage management

4.1 Super Twisting Sliding Mode Controller

First, we define an HSC current, I_HSC, which is derived by using KCL, to develop a suggested controller.

$$I_{HSC} = h_1 - \frac{h_2}{C} \tag{15}$$

The error z_1 is difference of I_{HSC} and I_{HSCref}.

$$z_1 = I_{HSC} - I_{HSCref} \tag{16}$$

where I_{HSCref} is the reference current for the HSC.

Putting I_{HSC} from equation (15) to (16) gives

$$z_1 = h_1 - \frac{h_2}{C} - I_{HSCref} \tag{17}$$

Now defining other two errors as

$$z_2 = h_2 - h_{2ref} \tag{18}$$

$$z_3 = h_3 - h_{3ref} \tag{19}$$

where h_{2ref} and h_{3ref} are the reference voltage values.

By taking derivative of equations $(17) - (19)$, where $I_{HSCref}^{\cdot}$, $h_{2ref}^{\cdot}$ and $h_{3ref}^{\cdot}$ are equal to zero.

$$\dot{z_1} = \dot{h_1} - \frac{\dot{h_2}}{C} \tag{20}$$

$$\dot{z_2} = \dot{h_2} \tag{21}$$

$$\dot{z_3} = \dot{h_3} \tag{22}$$

Now select the sliding surface ξ that permits system's states to chase their trajectories as:

$$\xi = g_1 z_1 + g_2 z_2 + g_3 z_3 \tag{23}$$

Where g_1, g_2 and g_3 are positive integer.

Derivative of equation (23) yields:

$$\dot{\xi} = g_1 \dot{z_1} + g_2 \dot{z_2} + g_3 \dot{z_3} \tag{24}$$

The Lyapunov candidate function is taken into consideration for the stability analysis as:

$$V = \frac{1}{2}\xi^2 \tag{25}$$

By taking time derivative of Eq. (25) gives:

$$\dot{V} = \xi\dot{\xi} \tag{26}$$

Putting the value of $\dot{\xi}$ from equation. (24) into equation (26)

$$\dot{V} = \xi(g_1\dot{z_1} + g_2\dot{z_2} + g_3\dot{z_3}) \tag{27}$$

Now substituting the values of $\dot{z_1}$, $\dot{z_2}$ and $\dot{z_3}$ from equations $(20) - (22)$ respectively, in Eq. (27), we have:

$$\dot{V} = \xi(g_1(\dot{h_1} - \frac{\dot{h_2}}{C}) + g_2\dot{z_2} + g_3\dot{z_3}) \tag{28}$$

The constraints are introduced to make $\dot{V}$ negative definite:

$$g_1\left(\dot{h_1} - \frac{\dot{h_2}}{C}\right) + g_2\dot{z_2} + g_3\dot{z_3} = -\beta_1|\xi|^{0.5}sign(\xi) - \int_0^t \beta_2\, sign(\xi)d\tau \tag{29}$$

Putting the value of $\dot{h_1}$ from equation (11) into equation (29), we have:

$$-\beta_1|\xi|^{0.5}sign(\xi) - \int_0^t \beta_2\, sign(\xi)d\tau = g_1\left(-\frac{R_i}{L_i}h_1 - \frac{1}{L_i}h_2 + \omega\frac{V_{DC}}{L_i} + d(t) - \frac{\dot{h_2}}{C}\right) + g_2\dot{z_2} + g_3\dot{z_3} \tag{30}$$

Now the overall controller U_{ST-SMC} can be obtained from equation (30) as:

$$U_{ST-SMC} = X(\frac{-g_1 R_i h_1}{L_i} - \frac{g_1 h_2}{L_i} + d(t) - \frac{g_1 \dot{h}_2}{C} + g_2 \dot{z}_2 + g_3 \dot{z}_3 + \beta_1 |\xi|^{0.5} sign(\xi) + \int_0^t \beta_2 \, sign(\xi) d\tau \tag{31}$$

Where

$$X = -\frac{L_i}{g_1 V_{DC}} \tag{32}$$

For the control, put $d(t) = 0$ in equation (31). The U_{eq} and U_{sw} can be obtained from equation (31):

$$U_{eq} = X(\frac{-g_1 R_i h_1}{L_i} - \frac{g_1 h_2}{L_i} - \frac{g_1 \dot{h}_2}{C} + g_2 \dot{z}_2 + g_3 \dot{z}_3) \tag{33}$$

And,

$$U_{sw} = X(\beta_1 |\xi|^{0.5} sign(\xi) + \int_0^t \beta_2 \, sign(\xi) d\tau) \tag{34}$$

$\beta_1, \beta_2, \lambda min, \lambda max$ and ρ are the design parameters which are given in [48] as:

$$\beta_2 > \frac{\rho}{\lambda_{min}} + B_2 \tag{35}$$

$$B_1{}^2 \geq \frac{4\rho \lambda_{max}(\beta_2 + \rho)}{\lambda_{min}{}^2 \lambda_{min}(\beta_2 - \rho)} + B_1 \tag{36}$$

With condition,

$$\rho > \left| \frac{d\dot{\xi}}{dt} + \frac{d\dot{\xi}}{dt} [f(x,t) + b(t)u(t) + d(t)] \right| \tag{37}$$

where $f(x,t)$ is the matrix of system and $b(t)$ is the matrix of input.

$$0 \leq \lambda_{min} \leq \left| \frac{d\dot{\xi}}{du} \right| \leq \lambda_{max} \tag{38}$$

Now equation (28) can be simplified as:

$$\dot{V} = -\beta_1 |\xi|^{1.5} sign(\xi) - \xi \beta_2 \int_0^t sign(\xi) d\tau \tag{39}$$

the values of β_1 and β_2 fulfil the demand of inequalities (35) and (36). It is clear from equation (39) that $\dot{V}$ is the negative definite, verifying the stability of the system.

4.2   Integral backstepping Sliding Mode Control

An integrative backstepping sliding mode controller has been built in this part. The comparable controller is created by multiplying the error term by integral action. To make it resistant to outside disturbances, a switching term would be included.

Putting the value of $\dot{h}_1$ from equation. (11) into equation (20) gives:

$$\dot{z}_1 = -\frac{R_i}{L_i}h_1 - \frac{1}{L_i}h_2 + \omega\frac{V_{DC}}{L_i} - \frac{\dot{h}_2}{C} \tag{40}$$

Now define the integrator term µ as:

$$\mu = \int_0^t (I_{HSC} - I_{HSCref})dt \tag{41}$$

By taking the time derivative of equation (41) yields

$$\dot{\mu} = I_{HSC} - I_{HSCref} \tag{42}$$

From equation (16) and (42), we get:

$$\dot{\mu} = z_1 \tag{43}$$

Lyapunov function for system stability is viewed as:

$$V_1 = \frac{1}{2}z_1{}^2 + \frac{v}{2}\mu^2 \tag{44}$$

Where v is positive integer that is constant.

By taking time derivative of Eq. (44) gives:

$$\dot{V}_1 = z_1\dot{z}_1 + v\mu z_1 \tag{45}$$

Putting value of $\dot{z}_1$ from Eq. (40) into Eq. (45) gives:

$$\dot{V}_1 = z_1(-\frac{R_i}{L_i}h_1 - \frac{1}{L_i}h_2 + \omega\frac{V_{DC}}{L_i} - \frac{\dot{h}_2}{C} + v\mu) \tag{46}$$

For the stability of the system, put:

$$-\frac{R_i}{L_i}h_1 - \frac{1}{L_i}h_2 + \omega\frac{V_{DC}}{L_i} - \frac{\dot{h}_2}{C} + v\mu = g_1z_1 \tag{47}$$

Where g_1 is a positive constant. Using equations (46) and (47) we have:

$$\dot{V}_1 = -g_1 z_1{}^2 \tag{48}$$

Eq. (48) shows that $\dot{V}_1$ is the negative definite. Virtual control $h_2 = \sigma$ can be obtained from Eq. (47) as:

$$\sigma = L_i \left(-\frac{R_i}{L_i} h_1 + \omega \frac{V_{DC}}{L_i} - \frac{\dot{h}_2}{C} + \nu\mu + g_1 z_1 \right) \tag{49}$$

By defining another error z_2 for chasing the state h_2 to σ as,

$$z_2 = h_2 - \sigma \tag{50}$$

Using the value of h_2 from equation (50) in equation (40) gives:

$$\dot{z}_1 = -\frac{R_i}{L_i} h_1 - \frac{z_2}{L_i} - \frac{\sigma}{L_i} + \omega \frac{V_{DC}}{L_i} - \frac{\dot{h}_2}{C} \tag{51}$$

Now substituting the value of σ from equation (49) into equation (48), as:

$$\dot{z}_1 = -\nu\mu - g_1 z_1 - \frac{z_2}{L_i} \tag{52}$$

Plugging the value of $\dot{z}_1$ from equation (52) into equation (45), we get V_1 as:

$$\dot{V}_1 = -g_1 z_1{}^2 - \frac{z_1 z_2}{L_i} \tag{53}$$

By taking time derivative of equation (50) as

$$\dot{z}_2 = \dot{h}_2 - \dot{\sigma} \tag{54}$$

By taking time derivative of equation (49) gives:

$$\dot{\sigma} = -R_i \dot{h}_1 + \dot{\omega} V_{DC} - L_i \frac{\ddot{h}_2}{C} + L_i \nu z_1 + L_i g_1 \dot{z}_1 \tag{55}$$

Plugging the value of $\dot{z}_1$ from equation (52) into equation (55), we get $\dot{\sigma}$ as:

$$\dot{\sigma} = -R_i \dot{h}_1 + \dot{\omega} V_{DC} - L_i \frac{\ddot{h}_2}{C} + L_i \nu z_1 + L_i g_1 \left(= -\nu\mu - g_1 z_1 - \frac{z_2}{L_i} \right) \tag{56}$$

The complete Lyapunov candidate function V_{11} is given as:

$$V_{11} = V_1 + \frac{1}{2}z_2{}^2 \tag{57}$$

By taking the derivative of equation (57) with respect to time:

$$\dot{V}_{11} = \dot{V}_1 + z_2\dot{z}_2 \tag{58}$$

Putting the value of V_1 from equation (53) in equation (58) gives:

$$\dot{V}_{11} = -g_1 z_1{}^2 + z_2(\dot{z}_2 - \frac{z_1}{L_i}) \tag{59}$$

Now by substituting:

$$\dot{z}_2 - \frac{z_1}{L_i} = -g_2 z_2 \tag{60}$$

where $a2$ is a positive integer that is constant.

Stability of system can be ensured by these equations (59) and (60) as:

$$\dot{V}_{11} = g_1 z_1{}^2 + g_2 z_2{}^2 \tag{61}$$

Plugging the value of $\dot{\sigma}$ from equation (56) in equation (54), we get $\dot{z}_2$ as:

$$\dot{z}_2 = \dot{h}_2 - R_i \dot{h}_1 + \dot{\omega} V_{DC} - L_i \frac{\ddot{h}_2}{C} + L_i v z_1 + L_i g_1(-v\mu - g_1 z_1 - \frac{z_2}{L_i}) \tag{62}$$

From equation (60) and (62), we get U_{eq} as:

$$\dot{U}_{eq} = \frac{1}{V_{DC}}\left(\dot{h}_2 - \left(R_i \dot{h}_1 + \dot{\omega} V_{DC} - L_i \frac{\ddot{h}_2}{C} + L_i v z_1 + L_i g_1\left(-v\mu - g_1 z_1 - \frac{z_2}{L_i}\right)\right) - \frac{z_1}{L_i} + g_2 z_2\right) \tag{63}$$

Switching term is added to increase the robustness of controller as:

$$U_{sw} = X sign(\xi) \tag{64}$$

where X is a positive integer that is constant

The complete control u is given as:

$$U = U_{eq} + U_{sw} \tag{65}$$

Where

$$U_{eq} = \int_0^t \dot{U}_{eq}\, dt \tag{66}$$

Now using the values of U_{eq} from equation (66) and us from equation (64) in equation (65), we get IBS-SMC control $U_{IBS-SMC}$ law as:

$$U_{eq} = \int_0^t \frac{1}{V_{DC}} \left(\dot{h_2} - \left(R_i \dot{h_1} + \dot{\omega} V_{DC} - L_i \frac{\ddot{h_2}}{C} + L_i v z_1 + L_i g_1 \left(-v\mu - g_1 z_1 - \frac{z_2}{L_i} \right) \right) - \frac{z_1}{L_i} + g_2 z_2 \right) dt - X sign(\xi) \tag{67}$$

4.3   Gain tuning using Grey Wolf Optimization

A population-based algorithm called Grey Wolf Optimisation (GWO) imitates the hunting style of grey wolves. [49]. GWO is suggested to be enhanced in [50] to provide a chaotic component that allows the algorithm to escape local optima and enhances search space exploration. Additionally, it has a dynamic search mechanism that changes the search method according to the problem's fitness landscape and current iteration number. The gains of the controller are tuned in this study using I-GWO to reduce the error function. To symbolise the alpha, beta, delta, and omega roles of the wolf pack, I-GWO uses four search agents. Each search agent's position in the population is initially initialised with one of the four possible solutions to the problem being optimised by the algorithm.

The search agents change their positions in the hierarchy based on their roles after being evaluated by the cost function. In this study, the following ITAE cost function is utilised to reduce the error term:

$$min\, F_i(s) \;=\; min \int t|s_i(e_i)|\, dt \tag{68}$$

where i=1,2

$F_i(s)$ is cost function, s_i is sliding surface, t is time and i is 1 or 2 for G2V and V2G respectively. Beta and delta wolves pursue the second and third most promising paths, respectively, while the alpha wolf seeks the most promising path. The omega wolf will randomly search in any direction.

The search goes on until a stopping requirement is satisfied, like achieving a predetermined number of iterations or a tolerable cost level. The search agent's position with the lowest cost value is the ultimate solution.

I-GWO is applied separately on both controllers to minimize the cost function given in equation (68). Fig. 4.1 and 4.2 demonstrate the optimization performance of algorithm by depicting the decreasing trend of cost value at different gains. Table [1] shows the optimal gain values for tuned G2V and V2G controllers along with their cost values.
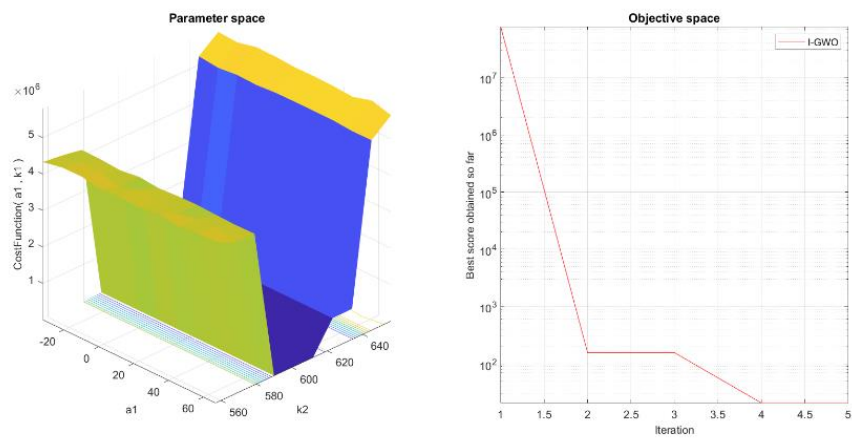
Figure 4. 1: G2V Optimization Results

Figure 4. 2: V2G Optimization Results
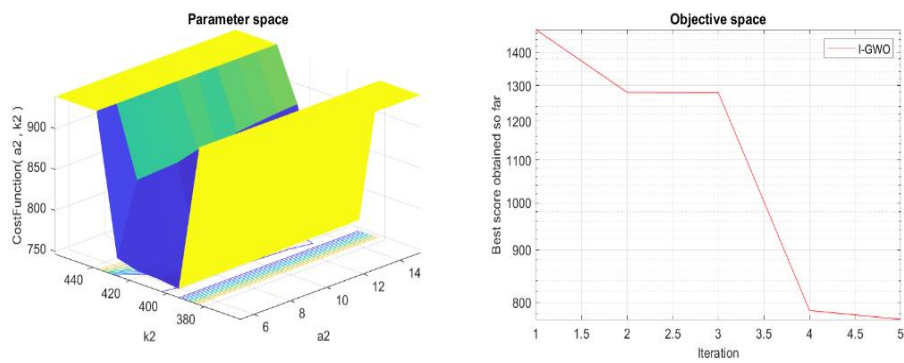
Table 1: Gain Results after Optimization

| Controller Gain	Value	Cost
g1 (G2V)	607.0315	20.734
g2 (G2V)	18.00082	
g1 (V2G)	410.7852	770.446
g2 (V2G)	10.264	

20

Chapter 5

5. Simulation and Results

The MATLAB/Simulink software has been used to validate the suggested controllers. Table 1 includes a list of the system parameters.

Table 2: The Circuit Components and their Values

Components	Values
Capacitor	700 µF
Inductance	5 mH
Resistance	0.1 Ω
Hybrid supercapacitor Capacitance	500 F
V_{DC}	400 V
Switching Frequency	20 KHz
Series Resistance	0.06 Ω

A disturbance of step-type has been introduced to the system before simulations in order to compare the performance of the developed controllers in both G2V and V2G modes of operation. The system's state x1 now includes the step disruption depicted in Fig. 8.
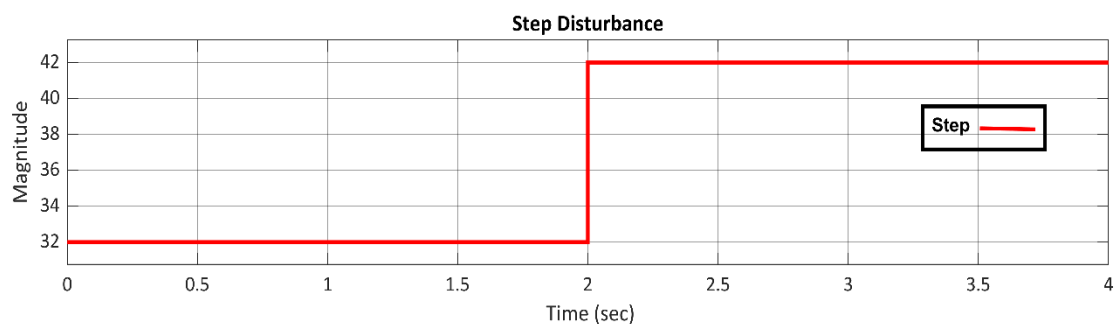
Figure 5. 1: Step

5.1   Simulation for G2V Mode

This section's goal is to demonstrate how the planned controllers behave in G2V mode of operation in face of disturbances. Figure 9 depicts the developed controllers' satisfactory performance in both stages the CC and CV stages using 230 V as the reference value for the HSC voltage. However, there is the significant amount of the chattering during IBS-SMC while there is hardly during ST-SMC.
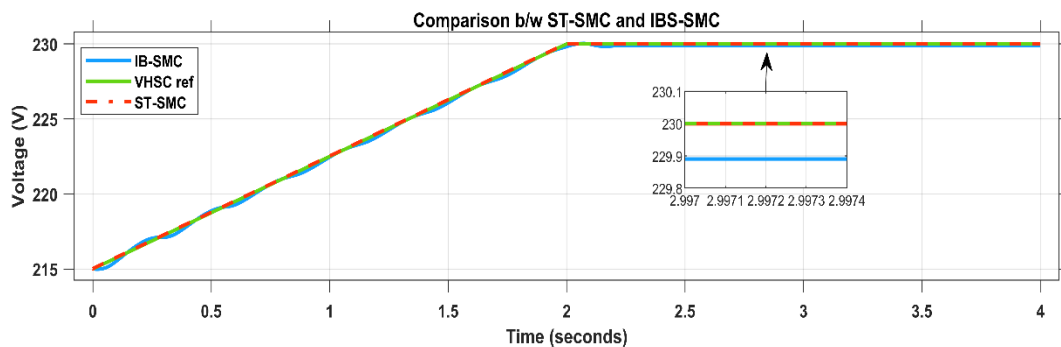

Figure 5. 2: HSC Voltage during G2V mode

Similar monitoring of the HSC current to the desired value of 10 A is shown in Fig. 10. In the CC stage, it can be shown that IBS-SMC exhibits significant steady state inaccuracy and chattering due to system disturbances, while ST-SMC exhibits superior chasing of the needed reference with less chattering. Fig. 11 displays the inner voltage of an HSC (V_C), which is a representation of its state of charge.
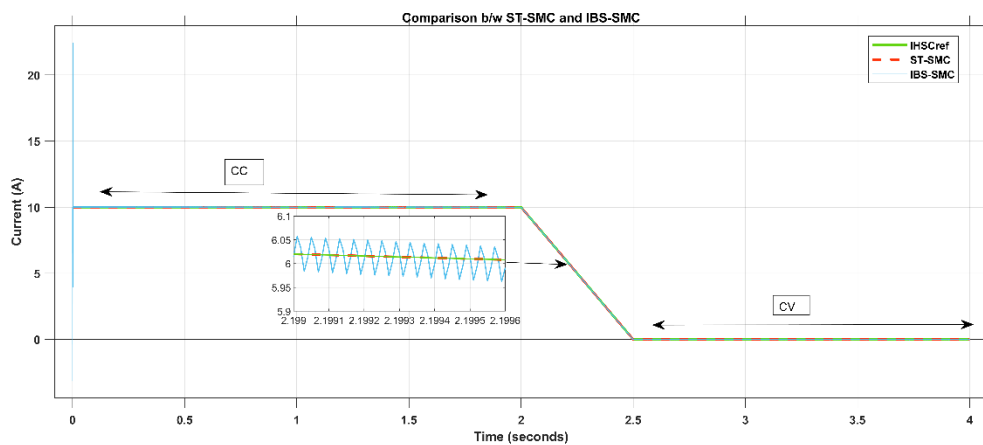

Figure 5. 3: HSC Current during G2V Mode

The inner voltage of an HSC (V_C) represents the state of charge of HSC and is shown in Fig. 11
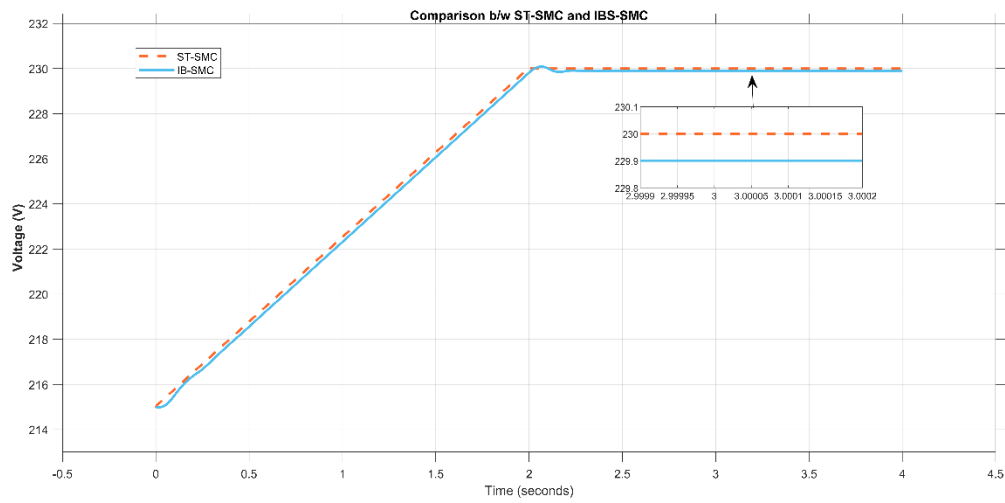
Figure 5. 4: HSC Inner Voltage in G2V

5.2 Simulation for V2G Mode

This part compares the presentation of both developed controllers in the V2G mode. The discharge of HSC utilizing only constant current (CC) stage and with the negative reference of 10 A is shown in Fig. 12. Both developed controllers can track the desired reference, but IBS-SMC exhibits far more chattering than ST-SMC does. Additionally, the IBS-SMC's high undershoot at delayed convergence weakens it because the system is already experiencing the effects of disruption.

Figure 5. 5: HSC Current during V2G Mode

23

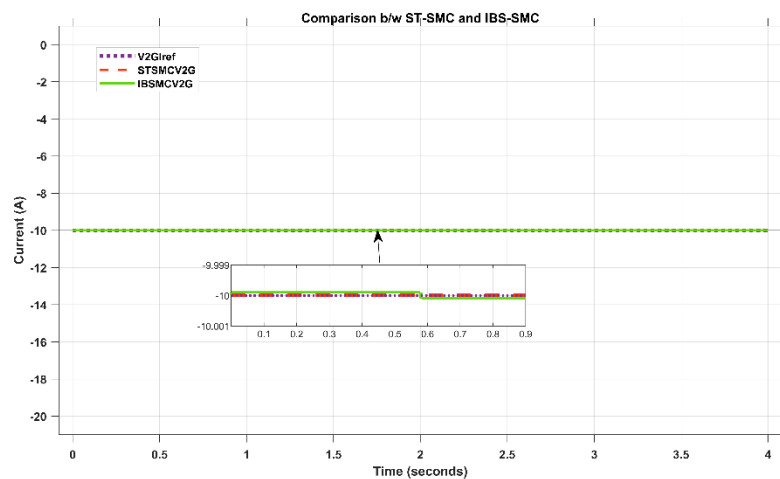The V_{HSC} and V_C of the HSC by both the developed controllers are shown in similar fashion in Figs. 13 and 14. The figures clearly show that the SoC of the HSC is quickly degrading during IBS-SMC, but the fast depleting of the HSC is being maintained during ST-SMC.
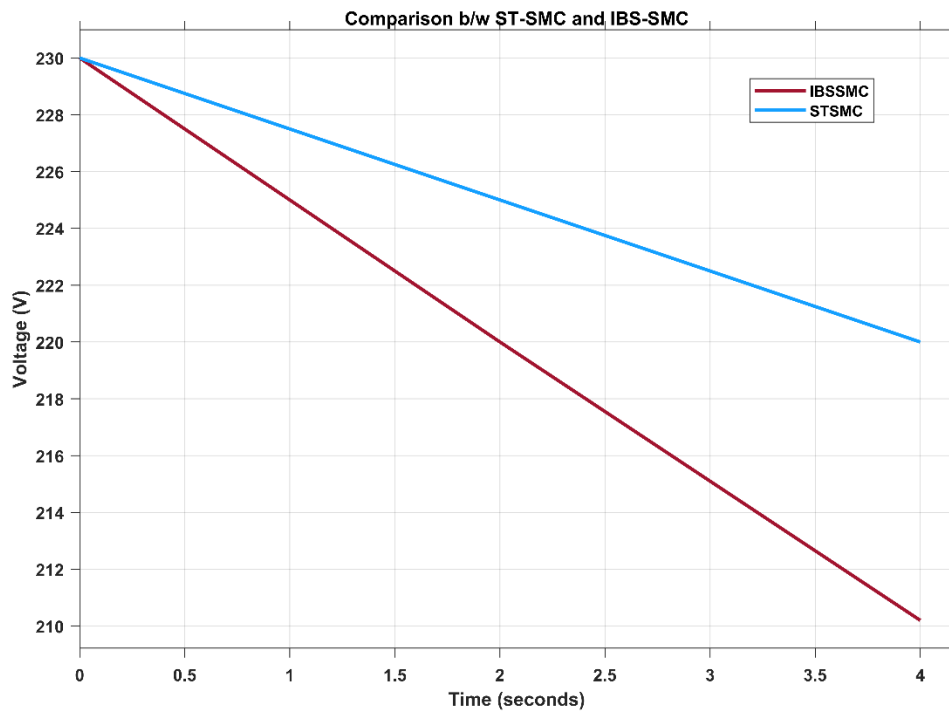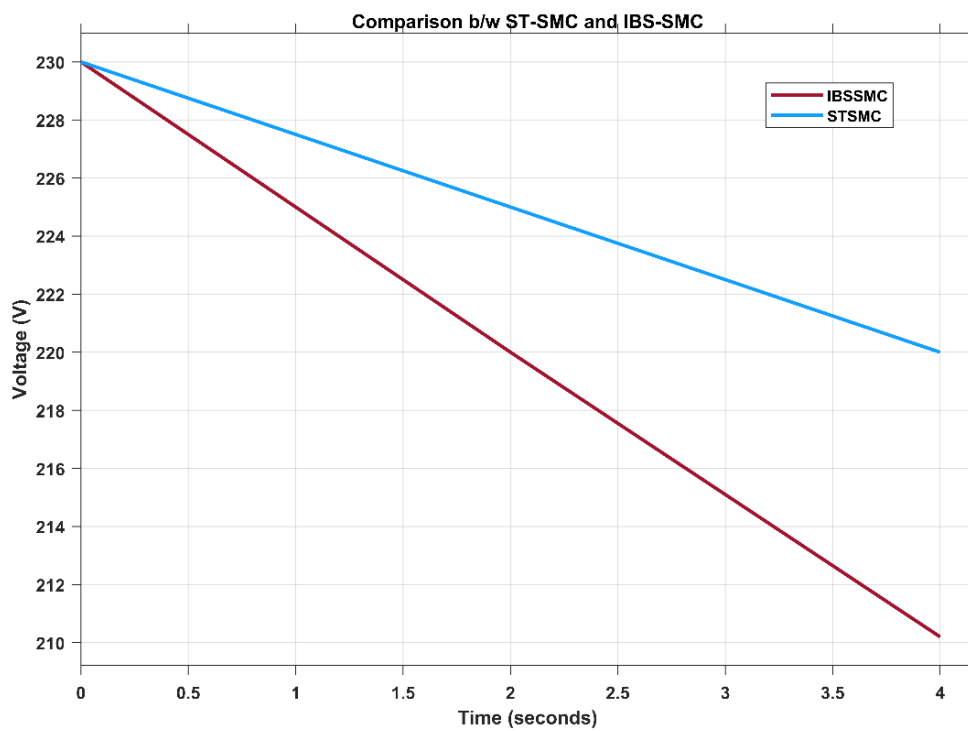

Figure 5. 6: HSC Voltage in V2G Mode

Figure 5. 7: HSC Inner Voltage V_C

5.3   Comparison between IBS-SMC and ST-SMC

In terms of their dynamic responsiveness, the developed controllers have also been assessed and contrasted, as quantitatively illustrated in Table (3). The ST-SMC's quick convergence to the target values may be shown by the fact that its settling time is lower than IBS-SMC's. Given that ST-SMC has a better transient response than IBS-SMC, the number of overshoots in the latter's instance is larger. Furthermore, the ST-SMC has a less steady state error than IBS-SMC, indicating the strong control even in face of disturbances in system. In the word, the ST-SMC surpasses IBS-SMC in nearly every area of dynamic responsiveness and exhibits greater robustness. The proposed system can be controlled robustly using ST-SMC because of all these aspects.

Table 3: Comparison of the dynamic performances of controllers

Response	ST-SMC	IBS-SMC
Rise Time	1.9002	1.9300
Settling Time	2.3439	2.3863
Overshoot	0.0024	0.0083
Undershoot	0.0	0.0
Peak Time	3.5973	3.5590
Peak Value	230.0042	230.0311
Steady Error	0.0022	0.022

Chapter 6

6 Conclusion

Control of the EV chargers in both operations G2V and V2G is proposed in this thesis work using an ST-SMC based controller. For comparison, the IBS-SMC has also been created for control of a charger's bi-directional converter. IBS-SMC performs well under dynamic conditions; however, it shows chattering effect, that results in system losses like heat and power. A super twisting algorithm-based controller is created to address this problem; it has superior dynamic performance than IBS-SMC and decreases the chattering effect. In comparison to the controller IBS-SMC, simulation results demonstrate quick convergence and less steady state error in the result of ST-SMC. The gain optimization is done by a good optimization technique. The grey wolf optimization technique has been done for gain optimization.

6.1 Future Work

Soon, EV chargers will be controlled by a variety of converters and control systems. It is also possible to research various combinations of energy sources. One of the upcoming works will also involve prototype validation.

Bibliography

[1] S. S. A. Y. a. J. Z. Brian Kihun Kim, "Electrochemical Supercapacitors for Energy Storageand Conversion," *Energy Systems,* 2015.

[2] C. BE, "Electrochemical supercapacitors," *Springer Science & Business Media,* 2013.

[3] P. H. L. G. M. K. Z. X. Chan CK, *Nat Nanotechnol,* pp. 331-35, 2008.

[4] H. K. Liu N, "Rice husks as a sustainable source of nanostructured silicon," *Sci Rep ,* 2013.

[5] G. Y. N. M. Simon P, pp. 845-54, 2008.

[6] B. O. V. J. H. H. El Brouji H, *Microelectron Relaibility,* no. 49, pp. 1391-7, 2009.

[7] B. E, "Development of lead-carbon hybrid battery/super capacitors," *Advance Capacitor World,* pp. 17-29, 2006.

[8] A. O. S.-G. J. M.-R. D. J. Gómez-Romero P, "Solid State electrochemical," no. 14, pp. 1939-45, 2010.

[9] C. Z. Z. W. S. X.] Lu Z, *Chemical communication,* no. 47, p. 9651–3, 2011.

[10] S. X. Z. N. X. K. Z. M. X. Y. Xie J, *Nano Energy,* no. 2, p. 65–74., 2013.

[11] P. S. Z. Y. A. J. R. R. Stoller MD, "Graphene-based ultracapacitors.," *Nano Lett,* no. 2, pp. 3498-502, 2008.

[12] Y. M. R. S. H. S. K. W. Akbulut S, *Application Electrochemical,* no. 47, pp. 1035-44, 2017.

[13] M. B. A. K. D. Aqib Muzaffar, "A review on recent advances in hybrid supercapacitors: Design, fabrication and application," *Renewable and Sustainable Energy Reviews,* no. 101, pp. 123-145, 2019.

[14] C. Chan, "The state of the art of electric, hybrid, and fuel cell vehicles," *Proceedings of the IEEE ,* vol. 4, no. 95, pp. 704-718, 2007.

[15] Z. A. Khaligh, " Battery, ultracapacitor, fuel cell, and hybrid energy storage systems for electric, hybrid electric, fuel cell, and plug-in hybrid electric vehiclestems for electric, hybrid electric,

fuel cell, and plug-in hybrid electric vehicles," *IEEE Trans. Veh. Technol.,* vol. 59, no. 6, p. 2806–2814, 2010.

[16] F. G. J. G. A. T. H. El Fadil, ", Modeling and nonlinear control of a fuel cell/supercapacitor hybrid energy storage system for electric vehicles," *IEEE Transaction of veh. Technol.,* vol. 63, no. 7, p. 3011–3018, 2014.

[17] V. R. R. C.-C. L. V. A. L. F. B. M. Carignano, "Assessment of energy management in a fuel cell/battery hybrid vehicle," *IEEE Access,* vol. 7, p. 16110–16122, 2019.

[18] M. K. Bauman, *IEEE Trans. Veh. Technol,* vol. 57, no. 2, p. 760–769, 2008.

[19] S. B. M. G. M. Rajabzadeh, "Dynamic modeling and nonlinear control of fuel cell vehicles with different hybrid power sources," *J. Hydrogen Energy,* vol. 41, no. 4, p. 3185–3198, 2016.

[20] F. B. A. R. F. G. T. A.-A. H. El Fadil, "Non-linear modelling and observer for supercapacitors in electric vehicle applications," *IFAC-Papers online,* vol. 1, no. 50, pp. 1898-1903, 2017.

[21] O. B. G. H. N. M. H. Al-Sheikh, "Power electronics interface configurations for hybrid energy storage in hybrid electric vehicles," in *17th IEEE Mediterranean Electrotechnical Conference*, MELECON, 2014.

[22] J. M. P. L. O. Hegazy, "Analysis, modeling, and implementation of a multidevice interleaved dc/dc converter for fuel cell hybrid electric vehicles," *IEEE Trans. Power Electronics,* vol. 27, no. 11, p. 4445–4458, 2012.

[23]]. J. Pinto, "Bidirectional battery charger with grid-to-vehicle, vehicle-to grid and vehicle-to-home technologies," in *IECON -39th Annual Conference of the IEEE*, 2013.

[24] H. M. M. A. I. A. S. A. R. Ijaz Ahmed, "Robust nonlinear control of battery electric vehicle charger in grid to vehicle and vehicle to grid applications," *Journal of Energy Storage,* no. 52, p. 104813, 2022.

[25] M. H. K. H. Y. I. T. Izumi, "Bidirectional charging unit for vehicle-to-X (V2X) power flow," *SEI Technical Revision,* no. 79, pp. 39-42, 2014.

[26] H. E. F. F. B. K. G. F. G. A. Rachid, "Lyapunov- based control of single-phase ac-dc power converter for BEV charger," in *3rd IEEE International Conference on Electrical and Information Technologies,ICEIT*, Rabat, Morocco, 2017.

[27] H. E. F. K. G. F. B. A. Rachid, "Output feedback control of bidirectional dc-dc power converter for BEV charger," in *4th International Conference on Automation, Control Engineering and ComputerScience, ACECS*, Morocco, 2017.

[28] A. K. J. Shen, "A supervisory energy management control strategy in a battery/ultracapacitor hybrid energy storage system," *IEEE Trans. Transp. Electrif,* vol. 1, no. 3, p. 223–231, 2015.

[29] N. A. P. Golchoubian, "Real-time nonlinear model predictive control of a battery–supercapacitor hybrid energy storage system in electric vehicles," *IEEE Trans. Veh. Technol,* vol. 66, no. 11, p. 9678–9688, 2017.

[30] I. A. H. A. N. A. M.S. Khan, "Backstepping sliding mode control of FC-UC based hybrid electric vehicle," *IEEE Access ,* no. 6, p. 77202–77211, 2018.

[31] Q. L. W. Y. W. Y. D. Xu, "Adaptive terminal sliding mode control for hybrid energy storage systems of fuel cell, battery and supercapacitor," *IEEE Access ,* vol. 7, p. 29295–29303, 2019.

[32] I. A. N. A. M. M. S. K. A. A. H. Armghan, "Nonlinear controller analysis of fuel cell–battery–ultracapacitor-based hybrid energy storage systems in electric vehicles," *Arab. J. Sci. Eng,* vol. 43, no. 6, pp. 3123–3133,, 2018.

[33] B. S. R. Pradhan, "Double integral sliding mode MPPT control of a photovoltaic system," *IEEE Trans. Control Syst. Technol,* vol. 24, no. 1, p. 285–292, 2016.

[34] I. A. Aqeel Ur Rahman, "Variable structure-based control of fuel cell-supercapacitor-battery based hybrid electric vehicle," *Journal of Energy Storage,* vol. 29, p. 101365, 2020.

[35] S. A. I. A. Hafiz Mian Muhammad Adil, "Control of MagLev system using supertwisting and integral backstepping sliding mode algorithim," *IEEE Access 8,* p. 51352–51362., 2020.

[36] H. E. F. K. G. F. B. A. Rachid, "Output feedback control of bidirectional dc-dc power converter for BEV charger," in *4th International Conference on Automation, Control Engineering and Computer Science, ACECS*, Tangier, Morocco, 2017.

[37] P. D. K. K. M. Karuppiah, "Design a electric vehicle charger based sepic topology with PI controller," in *IEEE International Conference on Advances and Developments in Electrical and Electronics Engineering,*, 2020.

[38] M. B. S. Devi Vidhya, "Hybrid fuzzy PI controlled multi-input DC/DC," *converter for electric vehicle application,* vol. 1, no. 61, p. 79–91., 2020.

[39] H. A. G. Khairy Sayed, "Electric vehicle to power grid integration using three-phase three-level AC/DC converter and PI-fuzzy controller," *Energies ,* vol. 9, no. 7, pp. 532-536, 2016.

[40] Chengqi, *IEEE J. ENergY,* 2021.

[41] A. Rachid, "Nonlinear output feedback control of V2G single phase on-board BEV charger," *Asian J. Control ,* vol. 5, no. 22, p. 1848–1859., 2020.

[42] I. A. S. A. H. A. I. Ahmed, "Robust nonlinear control of battery electric vehicle charger in grid to vehicle applications," *J. Energy Storage 42,* no. 42, p. 103039, 2021.

[43] S. Ahmed, "Conditioned-based robust nonlinear control of plug-in hybrid electric vehicle with saturated control actions," *Energy Storage ,* no. 43, p. 103201, 2021.

[44] Y.-M. L. K. T. C. Siew-Chong Tan, *IEEE Trans. 401 Ind. Electron,* vol. 3, no. 55, p. 1160–1174, 2008.

[45] W. L. J.J.E. Slotine, "Applied Nonlinear Control," in *Prentice-Hall*, Englewood Cliffs, 1991.

[46] V. Monteiro, "Assessment of a battery charger for electric vehicles with reactive power control," in *IECON 2012-38th Annual Conference on IEEE Industrial Electronics Society*, 2012.

[47] X. S. Y. A. X. Z. C. L. Xiaohu Zhang, "Design of a fast-charge lithium-ion capacitor pack for automated guided vehicle," *Journal of Energy Storage,* no. 48, p. 104045, 2022.

[48]]. C. Kunusch, "Sliding mode strategy for PEM fuel cells stacks breathing control using a super-twisting algorithm," *IEEE Trans. Control Syst. TechnolOGY,* vol. 1, no. 17, p. 167–174, 2008.

[49] S. Mirjalili, "Grey Wolf Optimizer," *Advances in Engineering Software,* vol. 69, pp. 46-61, 2014.

[50] M. H. Nadimi-Shahrak, "An improved grey wolf optimizer for solving engineering problems," *Expert Systems With Applications,* vol. 166, p. 113917, 2021.